Carbon 201 (2023) 900–909

Contents lists available at ScienceDirect

Carbon

journal homepage: www.elsevier.com/locate/carbon

# Blue, green and yellow carbon dots derived from pyrogenic carbon: Structure and fluorescence behaviour

C. Russo [a], A. Carpentieri [b], A. Tregrossi [a], A. Ciajolo [a], B. Apicella [a,*]

[a] Istituto di Scienze e Tecnologie per l'Energia e la Mobilità Sostenibili, CNR – P.le V. Tecchio, 80, 80125, Napoli, Italy
[b] Univ. Napoli Federico II, Dipartimento di Scienze Chimiche, Napoli, Italy

ARTICLE INFO

*Keywords:*
Fluorescence lifetimes
Carbon dots
PAHs
Organic carbon
Pyrogenic carbon
Soot
Mass spectrometry

ABSTRACT

Fluorescence lifetimes and quantum yields featuring polycyclic aromatic hydrocarbons (PAHs) and other organics constituting pyrogenic carbon particulate matter (PM) are seldom measured. In this work, PM sampled in a fuel-rich ethylene flame was firstly separated in organic carbon (OC), soluble in dichloromethane, and refractory organic carbon (ROC), soluble in *N*-methyl pyrrolidinone, and then analyzed by size exclusion chromatography (SEC) coupled with online UV and fluorescence detection, and by offline fluorescence spectroscopy and mass spectrometry. It was found that three classes of differently light emitting carbon dots (CDs) could be bottom-up synthesized in the same flame system by selecting appropriately the residence time. Actually, OC presented blue fluorescence regardless the residence time, whereas ROC sampled at low and high residence time emitted fluorescence in the green (green CDs) and in the yellow (yellow CDs) region, respectively. The SEC molecular weight of all CDs presented similar trimodal distributions, centered around 300, 1000 and 10,000 u. For the first time fluorescence lifetimes and quantum yields of pyrogenic CD fractions were measured as additional parameters useful for discriminating the fluorescent components and inferring their structural properties, with the support of mass spectrometry. The different spectroscopic features of CDs could be associated to different compositional characteristics as the polydispersity of molecular components featuring blue CDs, opposed to the oligomer-like nature of green and yellow CDs. Pyrogenic CDs showed different fluorescence emission ranges, quantum yield and lifetimes, appealing for their possible applications in the fields of imaging, electronics and sensors.

## 1. Introduction

The high sensitivity and selectivity of fluorescence spectroscopy toward aromatic molecules are useful for the detection of polycyclic aromatic hydrocarbons (PAHs). PAHs occurr naturally in fossil fuels and derived products, biomasses, and as trace contaminants in form of carbon particulate matter (PM) mainly emitted by pyrogenic processes and released in soils and aerosols [1,2]. Ex-situ fluorescence analysis of carbon PM [3] and their fractions [4] and in-situ laser induced fluorescence (LIF) [ [5] and references therein [6–8]] have been applied to pyrogenic PAHs for their identification and for inferring their role as intermediates in soot formation and emission and related health and climate effects. LIF is an online and non-intrusive technique used for the detection of differently-sized PAHs fluorescing in different emission wavelength regions [9–11]. The attribution to small and large PAHs of low (<400 nm) and high wavelength (>400–450 nm) fluorescence spectral regions, respectively, has been done by comparing in-situ and ex-situ measurements [3,12]; in these latter studies, visible emission has been attributed to the heavier part of organic carbon extracted/separated from PM. Recently, delayed fluorescence has been detected at high wavelengths and ascribed to PAH dimers [13,14].

Further interest on the fluorescence of pyrogenic PAHs derives from the recent positive perspective of PM as source of multiemissive nanocarbon materials like carbon dots (CDs), early detected in combustion-derived PM as oxidized candle soot [15,16] and in-flame soot [17–19]. CDs have attracted notable interest as promising competitors to semiconductor quantum dots and organic dyes due to their low toxicity, high biocompatibility and chemical stability [20–22]. These advantageous features have opened the route to diverse CD applications in various fields, ranging from imaging to sensing, photocatalysis, and energy conversion [23–27].

The first attempt to get CDs directly from soot, avoiding harsh

* Corresponding author.
*E-mail address:* barbara.apicella@stems.cnr.it (B. Apicella).

https://doi.org/10.1016/j.carbon.2022.09.062
Received 23 May 2022; Received in revised form 15 August 2022; Accepted 20 September 2022
Available online 28 September 2022

oxidative, expensive, and time-consuming treatments, has been done by Kumar et al., who analyzed the fluorescent behaviour of CDs derived from lamp soot in different solvents [28]. Blue-and green-emitting CDs have been recently extracted from flame soot without need of chemical post-treatments [19]. The green CDs presented quite excitation-independent fluorescence behaviour with low quantum yields (about 3%) [19]. Common to most of CDs derived from dehydration and thermal carbonization of carbon-based products, is the incomplete understanding of the fluorescence mechanism and the scarcity of information on the origin and the nature of fluorescence. The topic is very debated and all the proposed explanations can be summarized in three main emission mechanisms [29]: (1) the core emission, due to the conjugated π-domains of carbon core or to the quantum confinement effect [30,31]; (2) the surface states emission, related to the presence of functional groups connected with the carbon backbone [32]; and (3) the molecular state emission, originating from free or bonded fluorescent molecules [33,34]. In a previous work [19], the fluorescence of flame-formed CDs was hypothesised to be due to the carbon aromatic core whereas other authors found that the occurrence of surface functional groups and surface oxidation is a mechanism at the origin of CD fluorescence [35].

Following our previous work regarding blue and green CDs separated from PM sampled at low residence times of a fuel-rich laminar premixed ethylene flame [19], in the present work we have explored the same flame system and found the occurrence of yellow CDs just by sampling PM at high residence times. Deep insight on the fluorescence behaviour of these blue, green and yellow CDs in relation to their chemical structure is also given. More in detail, the PM fluorescing components were firstly separated in organic carbon (OC), soluble in dichloromethane (DCM) and in refractory organic carbon (ROC), soluble in *N*-methyl--pyrrolidinone (NMP). It is worth to note that most of CDs (e.g. those derived from citric acid) often contain highly fluorescent precursor molecules [33,34] and also in the present work blue-fluorescing PAH molecules, recognized as soot precursors and considered to mimic optical properties of CDs [36], have been found to be present in OC and, to a much lesser extent, in ROC. However, the high absorption in the visible of OC and ROC (corresponding to an optical band gap much lower than that of standard PAH and aromatic pitches [37]), TEM analysis (see Fig. 2 in Ref. 19) and size evaluation by size exclusion chromatography (SEC) hint to the CD nature of both OC (hereafter named blue CDs) and ROC (hereafter named yellow and green CDs), in dependence on their fluorescence emission. Blue, green and yellow CDs presented three MW-segregated fractions as separated in the 100-2E4 u range by SEC coupled with UV absorption and fluorescence detectors. Online fluorescence detection has been used for individuating the MW of main fluorophore class inside each CD class. In support to SEC and fluorescence measurements, CDs fractions, collected downstream SEC column, have been also individually analyzed by fluorescence spectroscopy and mass spectrometry.

Noteworthy, for the first time an important fluorescence parameter of CDs from pyrogenic carbon and of their fractions, namely the fluorescence lifetime, was provided as additional tool for inferring their structural properties, which in turn are important to disentangle their fluorescence mechanism [38] as well as their role as soot precursors and as health and climate altering.

## 2. Material and methods

### 2.1. Samples

Carbon PM was thermophoretically collected on glass plates [39] placed at 6 mm and 14 mm downstream of a premixed fuel-rich flame of ethylene/oxygen produced at atmospheric pressure on a commercial McKenna burner (Holthuis & Associates) (equivalence ratio = 3.03, velocity of 4 cm/s [40]). The two sampling points correspond to the beginning of soot formation region (young soot) and the region where soot formation attains the maximum concentration (mature soot), respectively. The experimental combustion system was described in detail elsewhere [40].

High purity solvents, standard PAHs as anthracene, phenanthrene, crysene, pyrene and coronene, blue and green graphene carbon dots and polyacenaphthylene (PACE) were purchased from Sigma Aldrich.

### 2.2. Separation and analysis

Carbon PM, caught on plates, was first extracted with DCM for separating OC soluble in DCM, from soot. NMP was used to achieve stable dispersions of soot to be analyzed by chromatographic and spectroscopic methods. Soot dispersions were further filtered on 20 nm pore size Anotop filters (Whatman), getting species with size <20 nm that are challenging and intriguing to be analyzed due to the low volatility and peculiar features as light absorption and emission in the visible [19]. These features have been attributed to heavy aromatic species so strongly incorporated in soot particles to require the use of a powerful solvent like NMP for their extraction. For this reason, such NMP-soluble soot fraction is here referred to as ROC [41].

The SEC separation of OC and ROC samples was carried out on a HPLC system HP1050 series by elution with NMP on a highly cross-linked "individual-pore" column (Polymer Laboratories, Ltd., U.K.; particle size of 5 μm diameter and a pore dimension of 50 nm), calibrated by external standard species (polystyrenes, PS) for MW determination in the 100 – 2E4 u range (corresponding to sizes of about 2–3 nm). The relation between retention times and molecular mass of PS has shown to be held also for PAH standards.

The species eluted from the SEC column were detected at the exit of the column by a HP1050 UV–Visible diode array detector, measuring the absorbance signal from 250 to 600 nm and a G1321AR fluorescence emission detector, placed in series to the UV–Visible detector. A delay time of 0.1 min was calculated between the UV–Visible and fluorescence detector and fluorescence emission chromatograms were accordingly shifted. Beside to get the MW distribution of OC and ROC, SEC was used to collect the three MW-segregated fractions of OC and ROC, separated on the basis of their chromatographic profiles, as described later on in the Results section.

UV–Visible and fluorescence emission spectra of OC and ROC and their MW-segregated fractions were measured in standard 1 cm pathlength quartz cells, on a HP8453 spectrophotometer and on a HORIBA Scientific FluoroMax-Plus TCSPC spectrofluorometer, respectively. The excitation source of the spectrofluorometer was a 150 W CW Ozone-free xenon arc lamp and the monochromators had Czerny-Turner design with plane gratings for optimized focus at all wavelengths and minimum stray light. The base detector was a Photomultiplier R928P, 185–900 nm, air cooled and stabilized.

The spectrofluorometer was equipped with an enhanced time correlated single photon counting (TCSPC) system with fast PPD fluorescence lifetime detector for very short (down to 25 ps) lifetime measurements. Two pulsed nanoLED (at 370 and 455 nm) were used as excitation sources. Decay Analysis Software (DAS) is used for deconvolving the decay curves.

Quantum yields (QY) were evaluated measuring the ratio between fluorescence and absorbance at a fixed wavelength by comparison with a standard species (9,10-diphenyl anthracene) [42].

Laser desorption ionization-time of flight mass spectrometry (LDI-TOFMS) was applied to OC and ROC samples and their fractions on positive reflectron mode on a SCIEX TOF/TOF™ 5800 System using a $N_2$ laser. The target was prepared by depositing on a standard stainless steel plate a sample dissolved/dispersed in NMP, without matrix, as all the investigated samples are able to absorb the light at the laser emission wavelength (337 nm), acting as a self-matrix [43–45]. Fast Fourier Transform (FFT) analysis was used to compute the discrete Fourier transform (DFT) of a repetitive signal like the intensity of mass spectrum peaks. A graphic software (Origin) has been used for mass spectrometry

data analysis. More details of LDI-TOFMS analysis and mass spectrometry data analysis are reported in Refs. [45,46].

## 3. Results

### 3.1. Steady-state fluorescence spectra and contour maps

The steady-state fluorescence spectra measured at selected excitation wavelengths and the contour maps of the 3D fluorescence spectra of OC and ROC are reported in Figs. 1–3 to give an overall view of their fluorescing properties. Consistently with the blue emission under UV light excitation (365 nm) (see the image in the inset of Fig. 2), the young OC emission spectra and related contour map show the maximum emission in the 425–500 nm emission wavelength range by using 300–350 nm excitation wavelength (contour map from red to yellow). OC sampling at different residence times along the flames presented very similar fluorescence behaviour with respect to young OC and the same blue light emission under UV light (365 nm). It is noteworthy that the fluorescence emission maximum of OC (red region in contour map) is localized in a very narrow emission wavelength range, 450–470 nm. Moreover, the emission spectra exhibit some fine structure in the spectral pattern, indicating the presence in OC of individual fluorescent molecules as PAHs and large PAHs [19]. In previous works, a mixture of three- and four-membered ring PAH was considered to mimic the optical properties of carbon dots, presenting a strong blue emission [47,48]. In the following, young and mature OC together will be hereafter grouped under the same name: blue CDs.

In comparison to OC fluorescence spectra, young ROC presents a broader fluorescence emission shifted at higher wavelengths, in the 480–640 nm range, by excitation in the 300–455 nm range (contour map from red to yellow) (Fig. 3). It can be also seen that young ROC produces visible emission in the green (see in the inset the image of the ROC solution under UV light (365 nm)). The broad and almost excitation-independent shape of fluorescence spectra of young ROC suggests a common fluorophore in ROC components. In the following, young ROC is named green CDs.

Interestingly, mature ROC exhibits a fluorescence spectral shape similar to that of young ROC, only slightly shifted at higher emission wavelengths (Fig. 3). This small downward shift corresponds to yellow light emission (see the image under UV light (365 nm) in the inset). Due to this characteristic, mature ROC is hereafter named yellow CDs.

### 3.2. MW distributions of blue, green and yellow CDs: absorption and fluorescence detection

Provided the aromatic nature of blue, green and yellow CDs separated by extraction of PM, the SEC analysis carried out in this work has shown to be effective in detecting all their components in a wide MW range (up to 2E4 u), when coupled with the UV–Visible detection. Specifically, the MW distributions based on the absorption fixed at 370 nm (upper part of Fig. 4), hereafter named absorption MW distributions, exhibit a multimodal distribution featured by three main MW modes, whose average MW values, reported on the peak apex in Fig. 4, are of the order of hundreds, thousand and tens of thousands mass units. The striking difference between the absorption MW distribution of blue CDs with respect to those of green and yellow CDs, is in the peak distribution ratio with the neat prevalence of the highest MW species mode (1.5E4 u) for green and yellow CDs (Fig. 4, middle and right) contrasted with the almost similar intensity of the three main peaks in the MW distribution of blue CDs (the lowest and the highest MW peak intensities are almost the same and the intermediate MW peak intensity is more than half of the others, Fig. 4, left). The slight shift toward higher MW of peak maxima of green and yellow CDs distribution is another signature of the larger high-MW species abundance in these samples.

Deep differences can be instead noticed in dependence on the detection system (absorbance or fluorescence), as shown in the lower part of Fig. 4, where the fluorescence MW distributions of CDs at two excitation wavelengths (370 and 455 nm) and fixed emission wavelength (500 nm) are reported. Actually, the fluorescence MW distribution appearance of all CDs (lower parts of Fig. 4) appears drastically modified in comparison to the absorption MW distributions. The almost complete disappearance of the highest MW mode is remarkable, denoting the overall negligible and/or low fluorescence of species with MW > 800-1000u. Moreover, in respect to the absorption MW distribution, the fluorescence MW distribution of blue CDs shows also a slight difference of the ratio between the peaks in the 100-1000u range with the large predominance of 100–400 u peak in respect to two smaller peaks at MW > 400 u, testifying the higher fluorescence of the first mode of MW distribution of blue CDs. As regards the effect of the excitation wavelength, the fluorescence MW distribution profile of blue CDs at higher excitation wavelength, $\lambda_{exc} = 455$ nm, presents the increase of the higher molecular mass peaks, hinting to some wavelength-dependence of blue CD fluorescence, associated to specific component features. By contrast, negligible wavelength dependence can be noticed for green and yellow CDs as deduced from the similarity of the fluorescence profiles at 370 and 455 nm excitation wavelength (lower part of Fig. 4).

The structural and optical properties of CDs have been more deeply investigated by analyzing the main MW-segregated fractions collected at the SEC column exit, in correspondence of the three main peaks indicated in Fig. 4. Even though the maxima of the fractions separated from the three samples are not located exactly at the same MW, for the sake of simplicity the fractions of CDs are hereafter named F-300 (the lighter fraction, with maximum at 260 u for blue CDs and 360 u for green and yellow CDs), F-1000 (the second fraction, with maximum at 750 u for blue CDs and 1300 u for green and yellow CDs), and F-10000 (the heavier fraction, with maximum at 10,000 u for blue CDs and 15,000 u

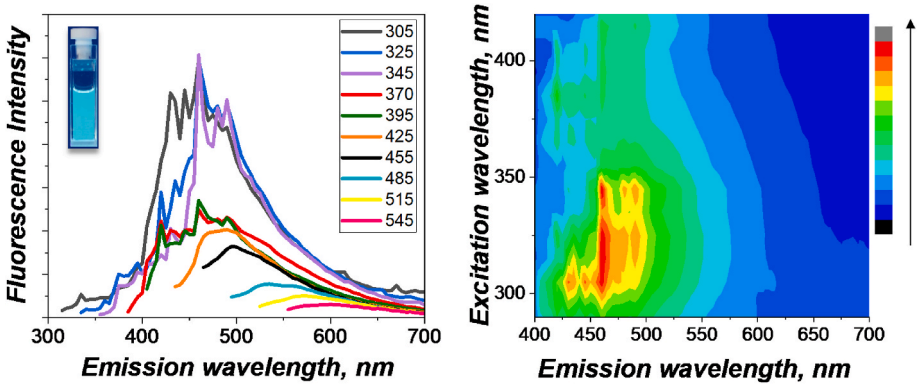


**Fig. 1.** OC (blue CDs): Emission spectra with 305–545 nm excitation wavelengths (left) and contour map of the three-dimensional fluorescence spectra (right). In the inset, the sample in NMP solution under UV light (365 nm). (A colour version of this figure can be viewed online.)

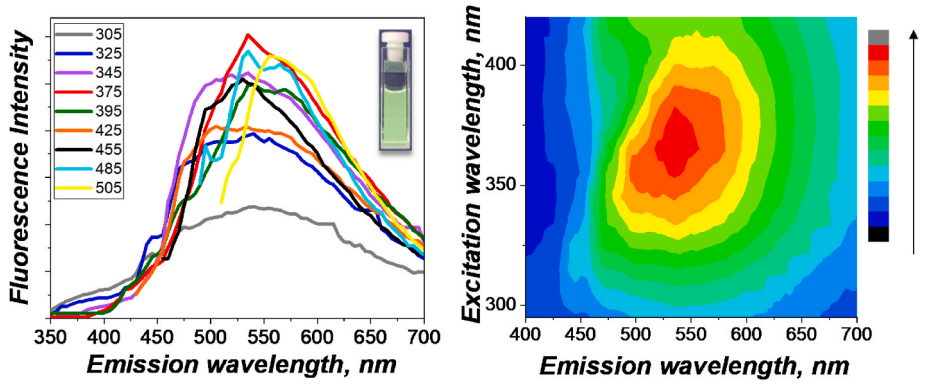


**Fig. 2.** Young ROC (green CDs): Emission spectra measured at 305–505 nm excitation wavelength (left) and contour map of the three-dimensional fluorescence spectra (right). In the inset, the sample in NMP solution under UV light (365 nm). (A colour version of this figure can be viewed online.)

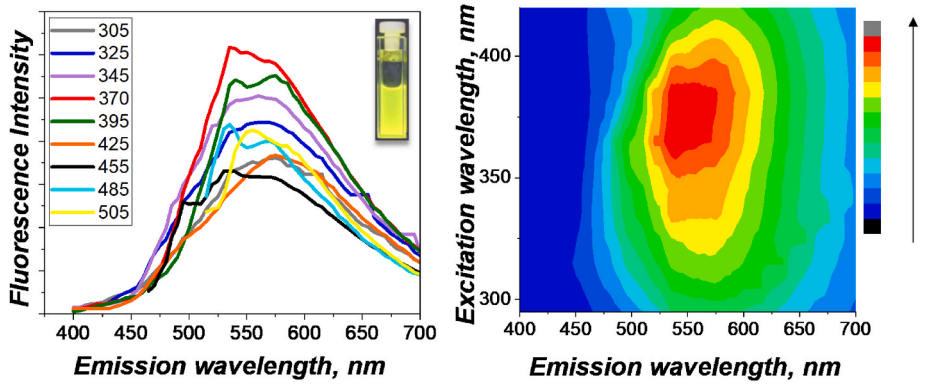


**Fig. 3.** Mature ROC (yellow CDs): Emission spectra at 305–505 nm at excitation wavelengths (left) and contour map of the three-dimensional fluorescence spectra (right). In the inset, the sample in NMP solution under UV light (365 nm). (A colour version of this figure can be viewed online.)

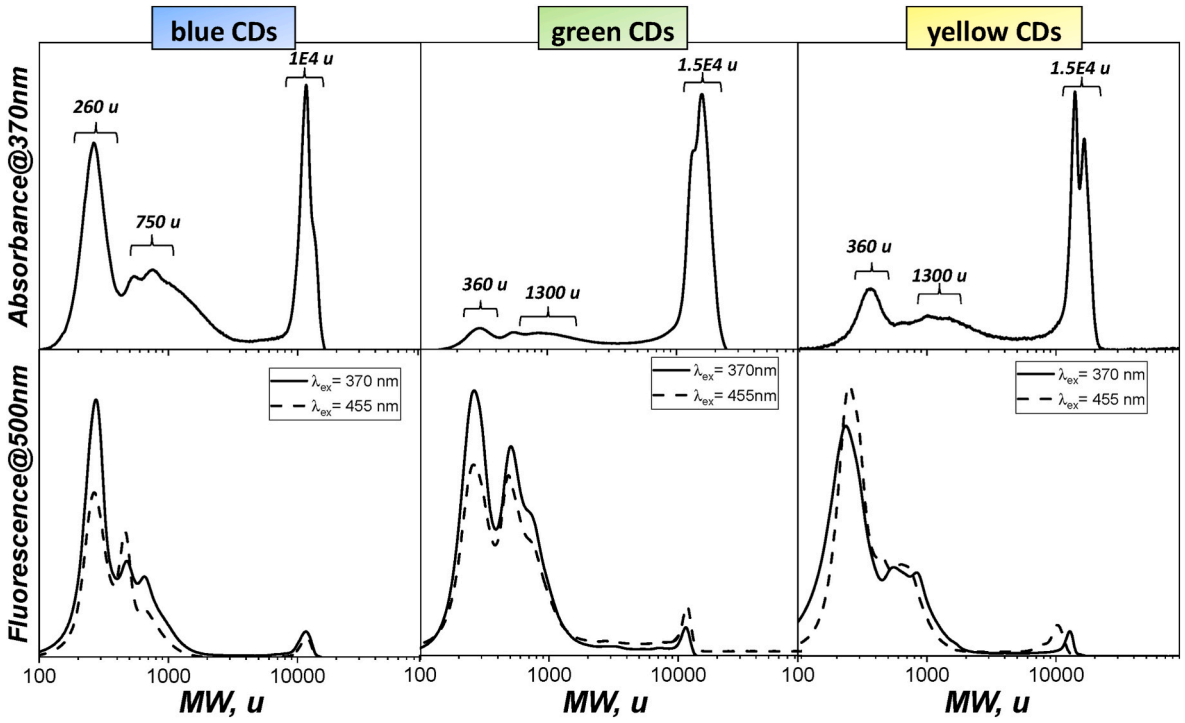


**Fig. 4.** MW distributions of blue CDs (left), green CDs (middle) and yellow CDs (right), acquired by SEC with UV–Visible detector at 370 nm (up) and fluorescence detector (down) at fixed emission wavelength (500 nm) by using 370 and 455 nm excitation wavelengths. (A colour version of this figure can be viewed online.)

for green and yellow CDs). The F-300-, F-1000 and F-10000 fractions, separated and collected downstream of the SEC column, were re-injected onto the same column to check the efficacy of SEC separation in terms of MW range selection. As matter of fact, the fluorescence MW distribution acquired for each fraction of CDs, reported in Fig. 5, is reduced to a single peak having fluorescence intensity that decreases going from the lighter up to heavier fractions. The bulk fluorescence spectra of CDs fractions, excited at 370 nm and reported in the inset of Fig. 5, show some fine structure traceable to individual PAHs, especially for F-300 and F-1000 of blue CDs and to some extent for F-300 of green CDs (Fig. 5 left and middle), whereas F-10000 of blue CDs, F-1000 and F-10000 of green CDs and yellow CDs fractions show a broad unstructured shape (Fig. 5).

The fluorescence spectra (height normalized) at $\lambda_{exc}$ = 370 nm of F-300 (left panel), F-1000 (middle panel) and F-10000 (right panel) fractions of blue, green and yellow CDs are contrasted in Fig. 6. The spectra clearly show the shift toward higher wavelengths passing from blue to green and yellow CDs, especially for F-300 and F-1000 fractions.

Thanks to the SEC separation, it has been also possible to measure the lifetime of each fraction useful for inferring the nature of fluorescing CDs components. The fluorescence decay profiles ($\lambda_{excitation}$ = 370 nm) of CDs and their MW/size segregated fractions are displayed in Fig. 7. It is worth to note that NMP, used as solvent, has higher viscosity (1.65cp @25 °C Sigma Aldrich) and lower oxygen solubility with respect of many other organic solvents [49] so reducing the oxygen quenching, known to affect lifetime measurements.

The decay of fluorescence intensity as a function of time in a uniform population of molecules excited with a brief pulse of light is described by an exponential function: $I(t) = Io \bullet \exp(-t/\tau)$, where I(t) is the fluorescence intensity measured at time t, Io is the initial intensity observed immediately after excitation, and $\tau$ is the fluorescence lifetime [11].

The fluorescence lifetime is the time that a molecule remains in an excited state prior to return to the ground state and it is characteristic for each fluorescent molecule. It is, however, also influenced by the chemical environment, i.e., the solvent characteristics. Indeed, during the excited state lifetime, a fluorophore can undergo conformational changes as well as interact with other molecules and diffuse through the local environment [42]. Complex systems, containing a mixed set of fluorophores, yield multi-exponential values [50] when fluorescence decay is measured, and an average value is generally evaluated [11]. The non-single exponential decay of fluorescence lifetimes, more than an indication of multiple contributions to the overall emission, can suggest also the occurrence of non-radiative pathways [29]. In the present work, three exponential components ($\tau_1$, $\tau_2$ and $\tau_3$) have been obtained by deconvolution of the fluorescence decays measured at $\lambda_{exc}$ = 370 and 455 nm, but the shorter lifetime ($\tau_1$ = 1.7 ns) due to NMP solvent, has been neglected. The exponential components attributable to the samples ($\tau_2$ and $\tau_3$) are reported in Table S1 in the Supplementary material, along with the pre-exponential factors. The average of $\tau_2$ and $\tau_3$, $\bar{\tau}$, reported in Table 1, lies in the 9–17 ns range at $\lambda_{exc}$ = 370 nm and 8–12 ns at $\lambda_{exc}$ = 455 nm. These lifetimes are shorter than those measured for PAHs like naphthalene and pyrene in cells at flame temperature [8] and also shorter than those measured in an opposed-flow flame [10]. However, they are comparable to lifetimes measured in the present work at ambient temperature in NMP ($\lambda_{exc}$ = 370 nm) for some 3–7 rings PAHs like anthracene, phenanthrene, crysene, pyrene and coronene (4–15 ns) and for commercial blue and green graphene carbon nanodots (15.7 and 4.6 ns, respectively). They are also consistent with the lifetimes of pyrolytic carbon solution measured at ambient temperature in different solvents and at similar excitation wavelengths [51,52]. Kumar and Bohidar [51] reported that the fluorescence lifetimes of pyrolytic carbon (see $\tau_2$ and $\tau_3$ in Ref. [51]) lie in the 5–19 ns range, which is similar to the ranges reported in Table S1. However, they have also evaluated a smaller average lifetime (3.5–7 ns) as the decay curves have been deconvolved with 3 parameters, but the first, very short, lifetime (see $\tau_1$, around 1 ns in Ref. [51]), due to solvent, was included in the average lifetime calculation. Carbon nanoparticles (3–4 nm diameter) prepared by microwave pyrolysis have shown comparable lifetimes of about 9 ns attributed to the radiative recombination nature of excitations [52].

The lifetime gives an absolute measure (independent of concentration) and allows a dynamic picture of the fluorescence, whereas steady-state fluorescence (emission intensity vs wavelength) provides an average representation. The fluorescence quantum yield ($\Phi$) of all fractions has been calculated from the steady-state fluorescence, as described in the experimental section and in Ref. [42], and reported in Table 1. The quantum yield of all CDs fractions exhibits a linear relationship with the average lifetime as shown in the diagram in Fig. 8. A linear trend between quantum yield and lifetime is rather common as the main relationship between quantum yield and lifetime is $\Phi = k_r \tau$ [11], where $k_r$ is the radiative constant rate. In the case of the CDs here studied, $k_r$ is of order of $10^7$ $sec^{-1}$, which is comparable for a similar spectral region with a strongly fluorescent organic dye like anthracene ($5*10^7$ $sec^{-1}$ [53]) and with the commercially supplied best-performing CdSe/ZnS QDs, "QD525PEG" from Invitrogen ($3*10^7$ $sec^{-1}$ [54]), suggesting the occurrence of very strong electronic transitions. It is noticeable that the lifetimes of green and yellow CDs fractions lie on the same line (Fig. 8) and their $k_r$ is about double with respect to the $k_r$ of blue CDs, which indicates a higher contribution of radiative with respect to non-radiative processes and therefore, better performances as CDs [55].

By reporting the quantum yields and lifetimes of CD fractions as a

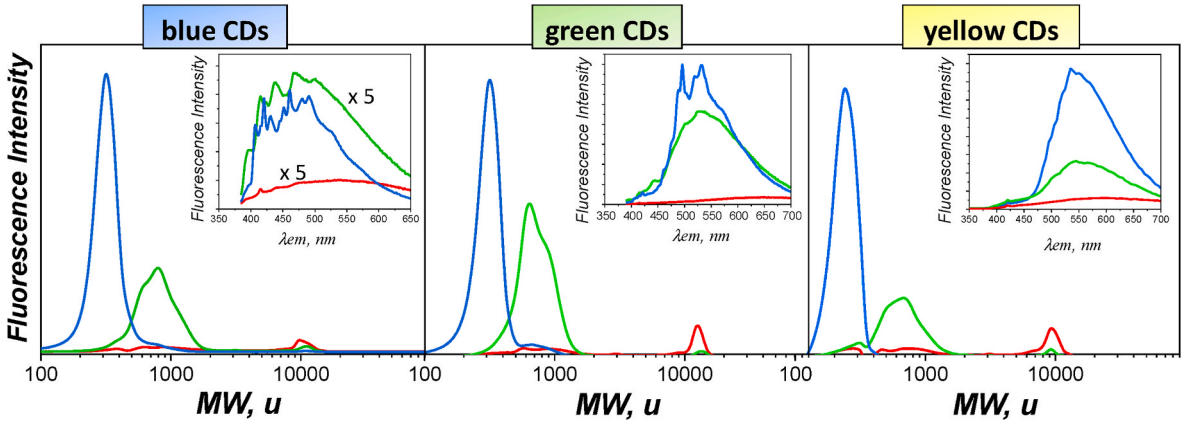


**Fig. 5.** MW distribution profiles of SEC separated fractions of blue (left), green (middle) and yellow (right) CDs, acquired with fluorescence detector at 370 nm excitation wavelength and 500 nm of emission wavelength. In the inset the emission fluorescence spectra at $\lambda_{exc}$ = 370 nm of the three fractions of CDs are reported. Blue line: F-300. Green line: F-1000. Red line: F-10000. (A colour version of this figure can be viewed online.)

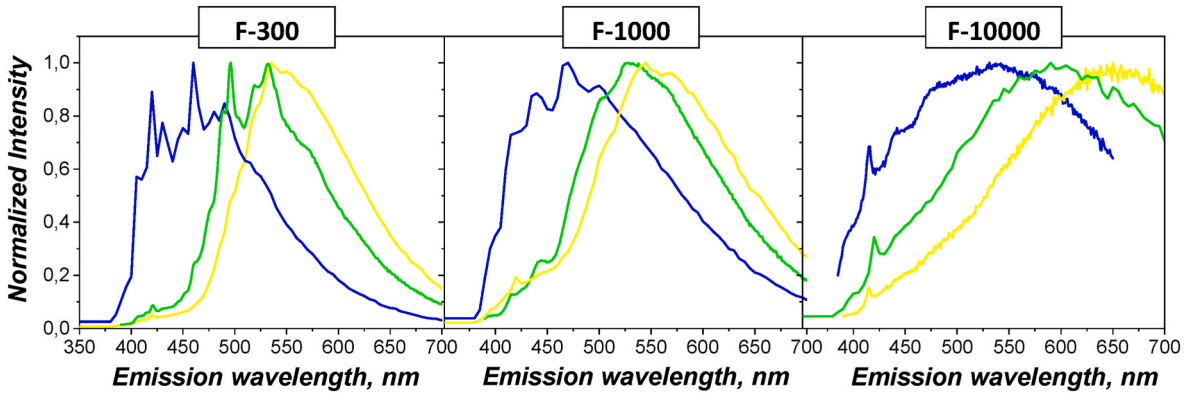


**Fig. 6.** Emission fluorescence spectra (height normalized) at $\lambda_{exc}$ = 370 nm of the three fractions of CDs. Blue line: Blue CDs. Green line: Green CDs. Yellow line: Yellow CDs. (A colour version of this figure can be viewed online.)

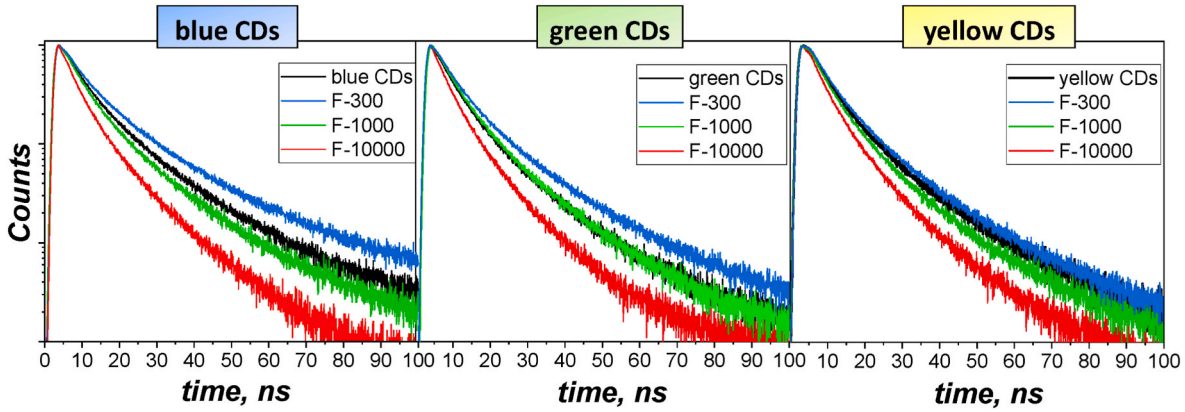


**Fig. 7.** Fluorescence decay curves of blue (left), green (middle) and yellow (right) CDs and their fractions at $\lambda_{exc}$ = 370 nm. (A colour version of this figure can be viewed online.)

**Table 1**
Average lifetimes and fluorescence quantum yield at 370 and 455 nm of CDs and their fractions.

| Samples | $\bar{\tau}_{370}$ (ns) | $\bar{\tau}_{455}$ (ns) | $\Phi_{370}$ (%) | $\Phi_{455}$ (%) |
|---|---|---|---|---|
| Blue CDs | 14.1 | 10.1 | 6.0 | 8.6E-02 |
| F-300 | 16.4 | 11.1 | 15.0 | 2.2E-01 |
| F-1000 | 11.8 | 9.3 | 7.0 | 1.0E-01 |
| F-10000 | 8.7 | 7,7 | 1.0 | 1.83E-02 |
| **Green CDs** | **10.7** | **9.5** | **3.4** | **4.3E-02** |
| F-300 | 12.6 | 11.9 | 23.0 | 3.4E-1 |
| F-1000 | 10.1 | 9.5 | 9.0 | 1.4E-1 |
| F-10000 | 8.3 | 7.7 | 9 E-2 | 2.0E-3 |
| **Yellow CDs** | **11.6** | **11.9** | **2.4** | **4.2E-02** |
| F-300 | 11.4 | 11.7 | 18.0 | 2.9E-01 |
| F-1000 | 10.6 | 10.9 | 12.0 | 2.0E-01 |
| F-10000 | 9.4 | 9.8 | 3.0E-1 | 9.5E-03 |

*the error on lifetimes was estimated to be ±0.3 ns.

function of MW in Figs. 9–11, their decrease with MW is well visualized both using $\lambda_{exc}$ = 370 nm and 455 nm. These trends hint to a relatively uniform fluorescence radiative process throughout the fractions [54], supposing that the variations observed in the quantum yield and lifetimes are mainly due to the non-radiative processes, which increase passing from a lighter fraction to a heavier one. The non-radiative processes, which are the sum of the internal conversion and intersystem crossing, appear to become more and more significant passing from lighter (F-300) to heavier components, almost completely overcoming radiative emission for F-10000. Moreover, lifetimes of blue CDs fractions significantly change when excitation wavelength changes

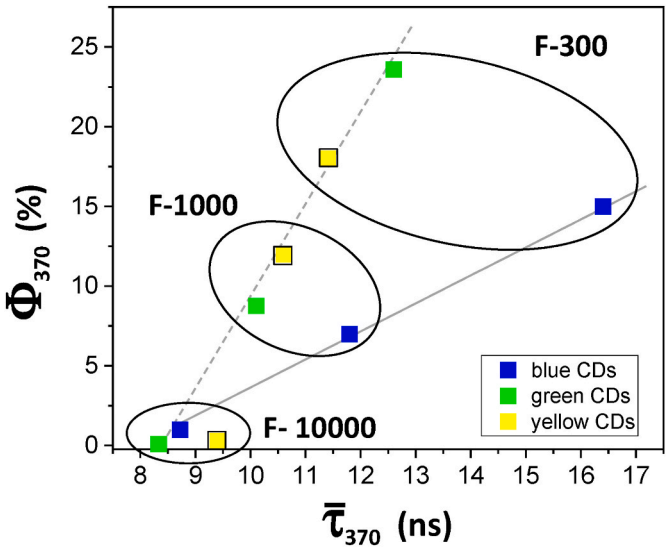


**Fig. 8.** Linear relationship between the quantum yields and average lifetimes for CD fractions at $\lambda_{exc}$ = 370 nm. The lines are only guide for eyes. (A colour version of this figure can be viewed online.)

(decreasing from $\lambda_{exc}$ = 370 to $\lambda_{exc}$ = 455 nm) (Fig. 9) and this feature confirms the polydispersity of blue CD fluorophores. Differently, the lifetimes for green and yellow CDs remain, in the error limit, unchanged (Figs. 10 and 11), supporting the macromolecular nature of these CDs,

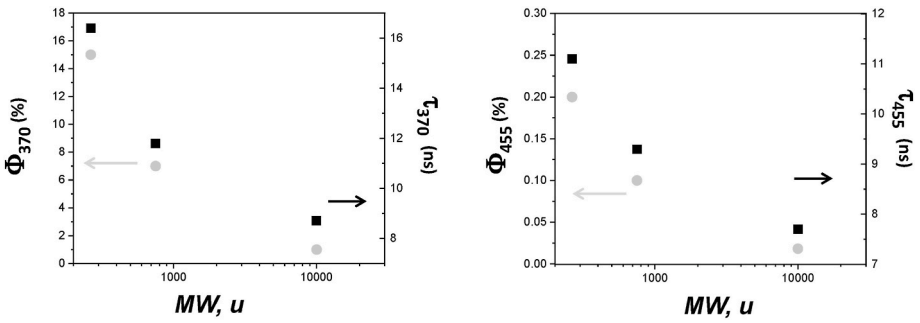


**Fig. 9.** Quantum yield (gray points) and lifetimes (black squares) of blue CDs fractions vs MW at $\lambda_{exc}$ = 370 nm (left) and 455 nm (right). (A colour version of this figure can be viewed online.)

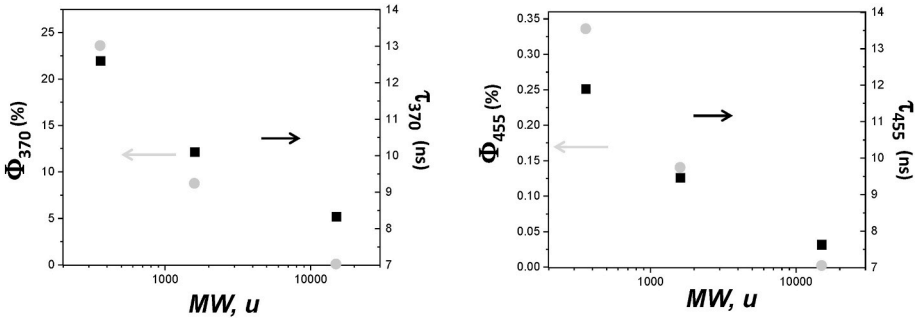


**Fig. 10.** Quantum yield (gray points) and lifetimes (black squares) of green CD fractions vs MW at 370 nm of excitation wavelength (left) and 455 nm (right). (A colour version of this figure can be viewed online.)

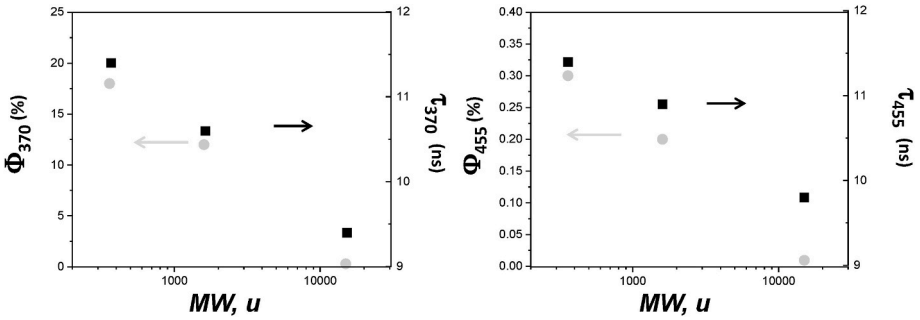


**Fig. 11.** Quantum yield (gray points) and lifetimes (black squares) of yellow CD fractions vs MW at 370 nm of excitation wavelength (left) and 455 nm (right). (A colour version of this figure can be viewed online.)

already presumed on the basis of the steady-state fluorescence spectra (Figs. 2 and 3).

As concerns the macromolecular character of green and yellow CDs, it can be underlined that the inverse proportionality of fluorescence quantum yield with MW has been typically found also for oligomers [56], and proposed as a method for calculating the degree of polymerization. The correlation of quantum yield and lifetimes with MW for PAH oligomers has been here verified for acenaphthene (ACE) and its oligomer, polyacenaphthylene (PACE) with a MW range of 5000–10,000 u.

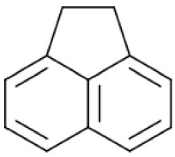

ACE

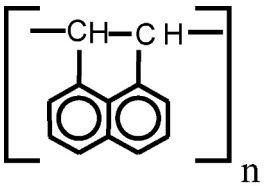


PACE

The features of both the UV–Visible absorption [57] and fluorescence spectra of ACE and PACE reported in the Supplementary material (Fig. S1) are very similar, demonstrating that the radiative process does not vary passing from acenaphthene to its oligomer PACE. This behaviour is explained by the fact that PACE is constituted of acenaphthene units linked by a single carbon–carbon bond, which avoids the conjugation between couples of adjacent rings and the consequent shift of absorption and fluorescence toward visible. It was found that, passing from the monomer to the polymer, the lifetime (at 370 nm of excitation

wavelength) decreases of about 20% (from 10.9 ns to 8.9 ns), whereas the quantum yield (at 300 nm of excitation wavelength) becomes less than a third (passing from 6.2% to 1.9%). Quantum yield was evaluated at 300 nm as at 370 nm absorption is too low, hindering quantum yield calculation.

Also in the case of green and yellow CDs, the similarity of fluorescence spectra of the fractions (Figs. 2 and 3), and the inverse proportionality of both fluorescence quantum yield and lifetimes with MW suggest that their fractions have a polymeric character with similar aromatic moieties (fluorophores) linked together by σ-bonds, interrupting bond conjugation. An easier energy dissipation through other conversion routes (roto-vibrational movements) is more probable for oligomers like PACE with respect to larger and more rigid or semi-rigid aromatic structures such as sandwich-like PAH structures [10]. For such polymer-like structure the probability for non-radiative decay increases with the MW increase, and the fluorescence quantum yield becomes lower and lower [58,59].

To support the interpretation of fluorescence behaviour hereafter reported, the MW composition of CDs fractions has been investigated by LDI-TOFMS. The spectra of F-300 and F-1000 of blue CDs, reported in Fig. S2 of the Supplementary material, have been analyzed by using FFT method evidencing periodic mass differences in the mass spectra [45,46]. To take into account for the change of the mass spectral distribution with increasing masses, the FFT analysis for green and yellow CDs has been carried out in selected mass ranges [45]. The FFT mass differences of CDs fractions are gathered in Table 2.

In the case of F-300 of blue CDs (Fig. S2 and Table 2), beside a mass spacing of 1 (indicating the presence of peaks at every mass unit), the 12 and 24 mass differences, typical of PAH growth sequences are noticed consistently with the polyaromatic nature of blue CDs. The F-1000 of blue CDs still presents the 12 and 24 peaks along with the 14 mass difference, indicative of methyl group substituents (also inside a ring) or methylene bridges between PAH units. The blue CDs mass spectrometric analysis has been reported in detail in a previous paper (see OC in Ref. [45]). In that paper, LDI-TOFMS at low and high laser power led to exclude the contribution of dimers and long chain alkyl-bridged PAHs, attributing the second mass spectral mode, corresponding to the F-1000 fraction of blue CDs, mainly to both fully-benzenoid and cyclopenta-PAHs. By analyzing the individual fractions, the interference of F-300 fraction composed of easily ionizable species (PAHs and large PAHs), which covers the signal of minor and less ionizable components, was avoided allowing to do some speculations about the structure of higher molecular weight fractions F-1000 and F-10000. In agreement with previous results [45], fluorescence analysis of the F-1000 fraction demonstrates that it is not constituted of PAH dimers (sandwich-like PAH structures or chemical bonded PAH dimers) as this kind of structures should exhibit a shift of the fluorescence emission and an increase of lifetimes [13,60]. It can be instead hypothesised that F-1000 is constituted mainly of cyclopenta-PAHs and large PAHs with aliphatic methylene bridges, which, interrupting conjugation, have the effect of decreasing lifetimes, without shifting the emission fluorescence range. However, also curved PAHs should be considered since the curvature decreases the lifetime, as found in the present work measuring the lifetimes of fullerenes with respect to large planar PAH (Tab. S2, Supplementary material) and in Refs. [61,62]. Curved PAH can be originated by the rearrangement of a PAH with an externally-fused cyclopenta group toward a PAH with a centrally-fused cyclopenta group, a process which has been observed under conditions pertinent to combustion [4,63,64].

**Table 2**
FFT mass difference for CDs and their MW-segregated fractions. (Bold numbers indicate the higher intensity peaks).

| Samples | mass range (m/z) | |
|---|---|---|
| | 200-1000 | |
| ***Blue CDs*** | 1, 12, 24 | |
| F-300 | 1, 12, 24 | |
| F-1000 | **1**, 12, 14, 24 | |
| F-10000 | 1, 12, 14 | |
| | **100-300** | **300-800** |
| ***Green CDs*** | 1,12, 14 | 1,12,24 |
| F-300 | - | 1, 12, 24 |
| F-1000 | 1, 12, 14 | **1**, 14, 24 |
| F-10000 | 1, 12, 14 | **1**, 14 |
| ***Yellow CDs*** | 1,12, 14 | 1, 12, 24 |
| F-300 | - | 1, 12, 24 |
| F-1000 | 1, 12, 14 | **1**, 14, 24 |
| F-10000 | 1, 12, 14 | **1**, 14 |

The F-10000 fraction of blue CDs presents 1, 12, 14 mass differences that can be due to the presence of homologous series of aromatic polymers (gap of $m/z$ 12) with a different degree of unsaturation (gap of $m/z$ 1) and aliphatic bridges ($CH_2$, gap $m/z$ 14).

F-300 of green and yellow CDs presents gaps similar to those found for F-300 of blue CDs (Table 2), but these gaps are found only above $m/z$ 300, indicating larger aromatic moieties with respect to F-300 of blue CDs (this is also confirmed by steady-state fluorescence spectra less structured and shifted at longer wavelengths, insets of Fig. 5).

F-1000 and F-10000 of green and yellow CDs are instead very similar but different from F-1000 of blue CDs. The mass differences of 1, 12 and 14, with prevalence of 1, support the attribution to polymers of aromatic monomers, linked by aliphatic bridges long enough to interrupt conjugation and leave unchanged the steady-state fluorescence (inset of Fig. 5).

## 4. Conclusions

The fluorescence features of pyrogenic PAHs and organic species constituting the extractable part of PM, sampled in fuel-rich ethylene premixed flame, have shown to be intriguing and challenging both for their structural elucidation and for exploring the promising applications of their fluorescence emitting performances. In the present work, the fluorescing PM components were discriminated firstly in OC and ROC classes, through separation in two different organic solvents, DCM and NMP, respectively. It was found that OC, coming from PM sampled at any residence time in flame, presents fluorescence emission in the blue region (420–500 nm), whereas ROC, derived from PM, sampled at low and high residence time, fluoresces in the green (500–550 nm) and yellow region (550–600 nm), respectively. Therefore, it has been demonstrated that it is possible bottom-up synthesizing three classes of CDs: blue, green and yellow CDs from the same flame system just by changing the solvent and selecting different residence time in the flame reactor.

The blue, yellow and green CDs have been analyzed by SEC coupled with online UV absorption and fluorescence detectors. Trimodal MW distributions, centered around 300, 1000 and 10,000 u, with different relative abundance for blue, yellow and green CDs have been observed. Specifically, high MW species were found to be more abundant in the green and yellow CDs.

The fluorescence lifetimes of blue, yellow and green CDs and their fractions as separated by SEC have been measured for the first time as additional tool for inferring their structural properties. It was found that the fluorescence lifetimes and quantum yield correlation with MW of CDs at different excitation wavelengths can give deep insights on their structure, furnishing a rapid and non-destructive screening for structural investigation of such complex materials. Blue CDs exhibit an excitation-dependent fluorescence, as well as a fine structure fluorescence pattern and lifetimes that present different trends with MW at different exciting wavelengths. Green and yellow CDs present almost excitation-independent spectra, with broad features, and almost constant lifetimes changing the emission wavelength.

SEC separation has allowed the isolation of MW-segregated fractions of these pyrogenic carbon CDs, individuating the MW range of species responsible for fluorescence emission. Fluorescence and mass spectrometric analysis data of the MW-segregated fractions separated from blue, green and yellow CDs have provided further insights on their structure also in relation to soot formation.

The following structures and emission mechanisms for CDs have been hypothesised: - a polydispersity of fluorescent molecular aromatic components for blue CDs, with a molecular state emission mechanism, originating from free or bonded fluorescent molecules; - whereas a macromolecular, oligomer-like nature for green and yellow CDs, with aromatic moieties linked by sigma-bonds, therefore with an emission mechanism as the core emission, due to the conjugated π-domains of carbon core. Blue, green and yellow CDs, here synthetized from pre-mixed flame PM without need of chemical post-treatments, present quantum yields and lifetimes typical of carbon dots, which make them appealing for application in the fields of imaging, electronics and sensors [65].

## CRediT authorship contribution statement

**C. Russo:** Conceptualization, Investigation, Data curation, Writing – review & editing, Supervision. **A. Carpentieri:** Investigation. **A. Tregrossi:** Investigation, Data curation. **A. Ciajolo:** Conceptualization, Writing – review & editing, Supervision. **B. Apicella:** Conceptualization, Writing – original draft, Investigation, Data curation, Writing – review & editing, Supervision.

## Declaration of competing interest

The authors declare that they have no known competing financial interests or personal relationships that could have appeared to influence the work reported in this paper.

## Acknowledgements

All authors acknowledge PRIN “Magic Dust” project 2017PJ5XXX for the financial support.

## Appendix A. Supplementary data

Supplementary data to this article can be found online at https://doi.org/10.1016/j.carbon.2022.09.062.

## References

[1] R. Niessner, W. Robers, A. Krupp, Detection of particulate polycyclic aromatic hydrocarbons by laser-induced time-resolved fluorescence, Fresenius’ J. Anal. Chem. 341 (1991) 207–213, https://doi.org/10.1007/BF00321550.
[2] K.C. Jones, J.A. Stratford, K.S. Waterhouse, N.B. Vogt, Organic contaminants in Welsh soils: polynuclear aromatic hydrocarbons, Environ. Sci. Technol. 23 (1989) 540–550, https://doi.org/10.1021/es00063a005.
[3] A. Ciajolo, B. Apicella, R. Barbella, A. Tregrossi, F. Beretta, C. Allouis, Depletion of fuel aromatic components and formation of aromatic species in a spray flame as characterized by fluorescence spectroscopy, Energy Fuels 15 (2001) 987–995, https://doi.org/10.1021/ef0100451.
[4] B. Apicella, R. Barbella, A. Ciajolo, A. Tregrossi, Comparative analysis of the structure of carbon materials relevant in combustion, Chemosphere 51 (2003) 1063–1069, https://doi.org/10.1016/S0045-6535(02)00715-4.
[5] P. Desgroux, X. Mercier, K.A. Thomson, Study of the formation of soot and its precursors in flames using optical diagnostics, Proc. Combust. Inst. 34 (2013) 1713–1738, https://doi.org/10.1016/j.proci.2012.09.004.
[6] H.A. Michelsen, Probing soot formation, chemical and physical evolution, and oxidation: a review of in situ diagnostic techniques and needs, Proc. Combust. Inst. 36 (2017) 717–735, https://doi.org/10.1016/j.proci.2016.08.027.
[7] M. Sirignano, D. Bartos, M. Conturso, M. Dunn, A. D’Anna, A.R. Masri, Detection of nanostructures and soot in laminar premixed flames, Combust. Flame 176 (2017) 299–308, https://doi.org/10.1016/j.combustflame.2016.10.009.
[8] F. Ossler, T. Metz, M. Alden, Picosecond laser-induced fluorescence from gas-phase polycyclic aromatic hydrocarbons at elevated temperatures. I. Cell measurements, Appl. Phys. B 72 (4) (2001) 465–478, https://doi.org/10.1007/s003400100519.
[9] A. Ciajolo, A. Tregrossi, R. Barbella, R. Ragucci, B. Apicella, M. de Joannon, The relation between ultraviolet-excited fluorescence spectroscopy and aromatic species formed in rich laminar ethylene flames, Combust. Flame 125 (2001) 1225–1229, https://doi.org/10.1016/S0010-2180(01)00242-5.
[10] M. Sirignano, A. Collina, M. Commodo, P. Minutolo, A. D’Anna, Detection of aromatic hydrocarbons and incipient particles in an opposed-flow flame of ethylene by spectral and time-resolved laser induced emission spectroscopy, Combust. Flame 159 (2012) 1663–1669, https://doi.org/10.1016/j.combustflame.2011.11.005.
[11] J.R. Lakowicz, Principles of Fluorescence Spectroscopy, second ed., Kluwer Academic/Plenum Publishers, New York, 1999.
[12] C. Allouis, B. Apicella, R. Barbella, A. Ciajolo, A. Tregrossi, Monitoring of fuel consumption and aromatics formation in a kerosene spray flame as characterized by fluorescence spectroscopy, Chemosphere 51 (2003) 1097–1102, https://doi.org/10.1016/S0045-6535(02)00712-9.
[13] S. Bejaoui, X. Mercier, P. Desgroux, E. Therssen, Laser induced fluorescence spectroscopy of aromatic species produced in atmospheric sooting flames using UV and visible excitation wavelengths, Combust. Flame 161 (2014) 2479–2491, https://doi.org/10.1016/j.combustflame.2014.03.014.
[14] X. Mercier, O. Carrivain, C. Irimiea, A. Faccinetto, E. Therssen, Dimers of polycyclic aromatic hydrocarbons: the missing pieces in the soot formation process, Phys. Chem. Chem. Phys. 21 (2019) 8285–8294, https://doi.org/10.1039/C9CP00394K.
[15] D. Saini, Gunture, J. Kaushik, R. Aggarwal, K.M. Tripathi, S.K. Sonkar, Carbon nanomaterials derived from black carbon soot: a review of materials and applications, ACS Appl. Nano Mater. 4 (12) (2021) 12825–12844, https://doi.org/10.1021/acsanm.1c02840.
[16] H. Liu, T. Ye, C. Mao, Fluorescent carbon nanoparticles derived from candle soot, Angew. Chem., Int. Ed. 46 (2007) 6473–6475, https://doi.org/10.1002/anie.200701271.
[17] X. Xu, R. Ray, Y. Gu, H.J. Ploehn, L. Gearheart, K. Raker, W.A. Scrivens, Electrophoretic analysis and purification of fluorescent single-walled carbon nanotube fragments, J. Am. Chem. Soc. 126 (2004) 12736–12737, https://doi.org/10.1021/ja040082h.
[18] Y.-P. Sun, B. Zhou, Y. Lin, W. Wang, K.A.S. Fernando, P. Pathak, M.J. Meziani, B. A. Harruff, X. Wang, H. Wang, P.G. Luo, H. Yang, M.E. Kose, B. Chen, L.M. Veca, S.-Y. Xie, Quantum-sized carbon dots for bright and colorful photoluminescence, J. Am. Chem. Soc. 128 (2006) 7756–7757, https://doi.org/10.1021/ja062677d.
[19] C. Russo, B. Apicella, A. Ciajolo, Blue and green luminescent carbon nanodots from controllable fuel-rich flame reactors, Sci. Rep. 9 (2019), 14566, https://doi.org/10.1038/s41598-019-50919-1.
[20] S.N. Baker, G.A. Baker, Luminescent carbon nanodots: emergent nanolights, Angew. Chem., Int. Ed. 49 (2010) 6726–6744, https://doi.org/10.1002/anie.200906623.
[21] H. Li, Z. Kang, Y. Liu, S.-T. Lee, Carbon nanodots: synthesis, properties and applications, J. Mater. Chem. 22 (2012) 24230–24253, https://doi.org/10.1039/C2JM34690G.
[22] M. Shamsipur, A. Barati, S. Karami, Long-wavelength, multicolor, and white-light emitting carbon-based dots: achievements made, challenges remaining, and applications, Carbon 124 (2017) 429–472, https://doi.org/10.1016/j.carbon.2017.08.072.
[23] R. Wang, K.-Q. Lu, Z.-R. Tang, Y.-J. Xu, Recent progress in carbon quantum dots: synthesis, properties and applications in photocatalysis, J. Mater. Chem. 5 (2017) 3717–3734, https://doi.org/10.1039/C6TA08660H.
[24] G.A.M. Hutton, B.C.M. Martindale, E. Reisner, Carbon dots as photosensitisers for solar-driven catalysis, Chem. Soc. Rev. 46 (2017) 6111–6123, https://doi.org/10.1039/C7CS00235A.
[25] H. Feng, Z. Qian, Functional carbon quantum dots: a versatile platform for chemosensing and biosensing, Chem. Rec. 18 (2018) 491–505, https://doi.org/10.1002/tcr.201700055.
[26] S.Y. Lim, W. Shen, Z. Gao, Carbon quantum dots and their applications, Chem. Soc. Rev. 44 (2015) 362–381, https://doi.org/10.1039/C4CS00269E.
[27] J. Wang, J. Qiu, A review of carbon dots in biological applications, J. Mater. Sci. 51 (2016) 4728–4738, https://doi.org/10.1007/s10853-016-9797-7.
[28] P. Kumar, H.B. Bohidar, Observation of fluorescence from non-functionalized carbon nanoparticles and its solvent dependent spectroscopy, J. Lumin. 141 (2013) 155–161, https://doi.org/10.1016/j.jlumin.2013.02.043.
[29] C.M. Carbonaro, R. Corpino, M. Salis, F. Mocci, S.V. Thakkar, C. Olla, P.C. Ricci, On the emission properties of carbon dots: reviewing data and discussing models, J Carbon research C 5 (2019) 60, https://doi.org/10.3390/c5040060.

[30] K.J. Mintz, Y. Zhou, R.M. Leblanc, Recent development of carbon quantum dots regarding their optical properties, photoluminescence mechanism, and core structure, Nanoscale 11 (2019) 4634–4652, https://doi.org/10.1039/C8NR10059D.
[31] H.J. Yoo, B.E. Kwak, D.H. Kim, Competition of the roles of π-conjugated domain between emission center and quenching origin in the photoluminescence of carbon dots depending on the interparticle separation, Carbon 183 (2021) 560–570, https://doi.org/10.1016/j.carbon.2021.07.054.
[32] S. Zhu, Y. Song, X. Zhao, J. Shao, J. Zhang, B. Yang, The photoluminescence mechanism in carbon dots (graphene quantum dots, carbon nanodots, and polymer dots): current state and future perspective, Nano Res. 8 (2015) 355–381, https://doi.org/10.1007/s12274-014-0644-3.
[33] J. Schneider, C.J. Reckmeier, Y. Xiong, M. von Seckendor, A.S. Susha, P. Kasak, A.-L. Rogach, Molecular fluorescence in citric acid-based carbon dots, J. Phys. Chem. C 121 (2017) 2014–2022, https://doi.org/10.1021/acs.jpcc.6b12519.
[34] W. Kasprzyk, T. Swiergosz, S. Bednarz, K. Walas, N.V. Bashmakova, D. Bogdał, Luminescence phenomena of carbon dots derived from citric acid and urea - a molecular insight, Nanoscale 10 (2018) 13889–13894, https://doi.org/10.1039/C8NR03602K.
[35] H. Ding, S.B. Yu, J.S. Wei, H.M. Xiong, Full-color light-emitting carbon dots with a surface-state-controlled luminescence mechanism, ACS Nano 10 (2016) 484–491, https://doi.org/10.1021/acsnano.5b05406.
[36] M. Fu, F. Ehrat, Y. Wang, K.Z. Milowska, C. Reckmeier, A. L Rogach, J. K Stolarczyk, A.S. Urban, J. Feldmann, Carbon dots: a unique fluorescent cocktail of polycyclic aromatic hydrocarbons, Nano Lett. 15 (9) (2015 Sep 9) 6030–6035, https://doi.org/10.1021/acs.nanolett.5b02215.
[37] C. Russo, B. Apicella, J.S. Lighty, A. Ciajolo, A. Tregrossi, Optical properties of organic carbon and soot produced in an inverse diffusion flame, Carbon 124 (2017) 372–379, https://doi.org/10.1016/j.carbon.2017.08.073.
[38] K.J. Mintz, M. Bartoli, M. Rovere, Y. Zhou, S.D. Hettiarachchi, S. Paudyal, J. Chen, J.B. Domena, P.Y. Liyanage, R. Sampson, D. Khadka, R.R. Pandey, S. Huang, C. C. Chusuei, A. Tagliaferro, R.M. Leblanc, A deep investigation into the structure of carbon dots, Carbon 173 (2021) 433–447, https://doi.org/10.1016/j.carbon.2020.11.017.
[39] C. Russo, B. Apicella, A. Tregrossi, M.M. Oliano, A. Ciajolo, Thermophoretic sampling of large PAH (C≥22–24) formed in flames, Fuel 263 (2020), 116722, https://doi.org/10.1016/j.fuel.2019.116722.
[40] B. Apicella, R. Barbella, A. Ciajolo, A. Tregrossi, Formation of low- and high-molecular-weight hydrocarbon species in sooting ethylene flames, Combust. Sci. Technol. 174 (2002) 309–324, https://doi.org/10.1080/713712948.
[41] V.B. Malmborg, A.C. Eriksson, S. Török, Y. Zhang, K. Kling, J. Martinsson, E. C. Fortner, L. Gren, S. Kook, T.B. Onasch, P.E. Bengtsson, J. Pagels, Relating aerosol mass spectra to composition and nanostructure of soot particles, Carbon 142 (2019) 535–546, https://doi.org/10.1016/j.carbon.2018.10.072.
[42] I.B. Berlman, Handbook of Fluorescence Spectra of Aromatic Molecules, Academic Press, New York, 1971.
[43] L. Przybilla, J.D. Brand, K. Yoshimura, H.J. Rader, K. Mullen, MALDI-TOF mass spectrometry of insoluble giant polycyclic aromatic hydrocarbons by a new method of sample preparation, Anal. Chem. 72 (2000) 4591–4597, https://doi.org/10.1021/ac000372q.
[44] B. Apicella, A. Carpentieri, M. Alfè, R. Barbella, A. Tregrossi, P. Pucci, A. Ciajolo, Mass spectrometric analysis of large PAH in a fuel-rich ethylene flame, Proc. Combust. Inst. 31 (2007) 547–553, https://doi.org/10.1016/j.proci.2006.08.014.
[45] B. Apicella, C. Russo, A. Carpentieri, A. Tregrossi, A. Ciajolo, PAHs and fullerenes as structural and compositional motifs tracing and distinguishing organic carbon from soot, Fuel 309 (2022), 122356, https://doi.org/10.1016/j.fuel.2021.122356.
[46] B. Apicella, A. Bruno, X. Wang, N. Spinelli, Fast Fourier Transform and autocorrelation function for the analysis of complex mass spectra, Int. J. Mass Spectrom. 338 (2013) 30–38, https://doi.org/10.1016/j.ijms.2013.01.003.
[47] M. Fu, F. Ehrat, Y. Wang, K.Z. Milowska, C. Reckmeier, A.L. Rogach, J. K. Stolarczyk, A.S. Urban, J. Feldmann, Nano Lett. 15 (2015) 6030–6035, https://doi.org/10.1021/acs.nanolett.5b02215.
[48] F. Ehrat, S. Bhattacharyya, J. Schneider, A. Löf, R. Wyrwich, A.L. Rogach, J. K. Stolarczyk, A.S. Urban, J. Feldmann, Nano Lett. 17 (2017) 7710–7716, https://doi.org/10.1021/acs.nanolett.7b03863.
[49] T. Sato, Y. Hamada, M. Sumikawa, S. Araki, H. Yamamoto, Solubility of oxygen in organic solvents and calculation of the hansen solubility parameters of oxygen, Ind. Eng. Chem. Res. 53 (49) (2014) 19331–19337, https://doi.org/10.1021/ie502386t.
[50] A. Sciortino, A. Cannizzo, F. Messina, Carbon nanodots: a review—from the current understanding of the fundamental photophysics to the full control of the optical response, Chimia 4 (2018) 67, https://doi.org/10.3390/c4040067.
[51] P. Kumar, H.B. Bohidar, Physical and fluorescent characteristics of nonfunctionalized carbon nanoparticles from candle soot, J. Nano Res. 14 (2012) 948, https://doi.org/10.1007/s11051-012-0948-8.
[52] H. Zhu, X. Wang, Y. Li, Z. Wang, F. Wang, X. Yang, Microwave synthesis of fluorescent carbon nanoparticles with electro-chemiluminescence properties, Chem. Commun. 34 (2019) 5118–5120, https://doi.org/10.1039/B907612C.
[53] N.J. Turro, Modern Molecular Photochemistry, University Science Books, Sausalito, CA, 1991.
[54] X. Wang, L. Cao, S.-T. Yang, F. Lu, M.J. Meziani, L. Tian, K.W. Sun, M. A. Bloodgood, Y.-P. Sun, Bandgap-like strong fluorescence in functionalized carbon nanoparticles, Angew. Chem. Int. Ed. 49 (2010) 5310–5314, https://doi.org/10.1002/anie.201000982.
[55] H. Liu, Z. Li, Y. Sun, X. Geng, Y. Hu, H. Meng, J. Ge, L. Qu, Synthesis of luminescent carbon dots with ultrahigh quantum yield and inherent folate receptor-positive cancer cell targetability, Sci. Rep. 8 (2018) 1086, https://doi.org/10.1038/s41598-018-19373-3.
[56] D. Cho, W.L. Mattice, L.J. Porter, R.W. Hemingway, Use of the fluorescence quantum yield for the determination of the number-average molecular weight of polymers of epicatechin with 4β→8 interflavan bonds, Polymer 30 (1989) 1955–1958, https://doi.org/10.1016/0032-3861(89)90277-2.
[57] B. Apicella, M. Alfè, R. Barbella, A. Tregrossi, A. Ciajolo, Aromatic structures of carbonaceous materials and soot inferred by spectroscopic analysis, Carbon 42 (2004) 1583–1589, https://doi.org/10.1016/j.carbon.2004.02.010.
[58] R.L. Vander Wal, K.A. Jensen, M.Y. Choi, Simultaneous laser-induced emission of soot and polycyclic aromatic hydrocarbons within a gas-jet diffusion flame, Combust. Flame 109 (1997) 399–414, https://doi.org/10.1016/S0010-2180(96)00189-7.
[59] R.L. Vander Wal, Soot precursor material: visualization via simultaneous lIF-LII and characterization via tem, Proc. Combust. Inst. 26 (1996) 2269–2275, https://doi.org/10.1016/S0082-0784(96)80054-3.
[60] H. Saigusa, E.C. Lim, Pump-probe fluorescence studies of excimer formation and dissociation for the van der Waals dimer of fluorine, J. Phys. Chem. 95 (6) (1991) 2364–2370, https://doi.org/10.1021/j100159a046.
[61] Q. Xu, C. Wang, Y. Zhao, D. Zheng, C. Shao, W. Guo, X. Deng, Y. Wang, X. Chen, J. Zhu, H. Jiang, Tuning the properties of corannulene-based polycyclic aromatic hydrocarbons by varying the fusing positions of corannulene, Org. Lett. 22 (18) (2020) 7397–7402, https://doi.org/10.1021/acs.orglett.0c02754.
[62] J. Dey, A. Will, R.A. Agbaria, P.W. Rabideau, A.H. Abdourazak, R. Sygula, I. M. Warner, Spectroscopic study of a representative polar cap of buckminsterfullerene: Cyclopentacorannulene, J. Fluoresc. 7 (3) (1997) 231–236, https://doi.org/10.1007/BF02758223.
[63] L.T. Scott, Fragments of fullerenes: novel syntheses, structures and reactions, Pure Appl. Chem. 68 (2) (1996) 291–300, https://doi.org/10.1351/pac199668020291.
[64] A.L. Lafleur, J.B. Howard, K. Taghizadeh, E.F. Plummer, L.T. Scott, A. Necula, K. C. Swallow, Identification of C20H10 dicyclopentapyrenes in flames: correlation with corannulene and fullerene formation, J. Phys. Chem. 100 (1996) 17421–17428, https://doi.org/10.1021/jp9605313.
[65] L. Cao, M. Zan, F. Chen, X. Kou, Y. Liu, P. Wang, Q. Mei, Z. Hou, W.-F. Dong, L. Li, Formation mechanism of carbon dots: from chemical structures to fluorescent behaviors, Carbon 194 (2022) 42–51, https://doi.org/10.1016/j.carbon.2022.03.058.